HIGH CORRELATION BETWEEN HADDOCKING SCORE AND SMD RUPTURE FORCE IN *i*BRAB FAB MODEL AND IAV HA PROTEIN SYSTEMS

Do N.P. Chau[1,2]

[1] *School of Biotechnology, International University, HCMC, Vietnam*
[2] *Vietnam National University, Hochiminh City, Vietnam*

ABSTRACT

Therapeutic monoclonal antibodies represent a potent strategy for combating acute infectious diseases. However, identifying the most efficacious antibodies among the vast human variants necessitates extensive time and advanced technological resources. The iBRAB method, previously introduced, aims to harness studied antibodies to engineer a broad-spectrum antibody capable of neutralizing antigens from diverse strains of Influenza A virus. Initially, we assessed the predictive performance of HADDOCK in delineating binding configurations across a range of protein complexes. This investigation again delves into the intricate interplay between computational docking forecasts and the mechanical resilience of protein-protein interactions by utilizing the iBRAB method in conjunction with Steered Molecular Dynamics (SMD) simulations. Emphasis was placed on optimizing pulling parameters, such as force and rate, within SMD simulations to ensure the fidelity of rupture force measurements. Our findings reveal a robust positive correlation between the docking scores forecasted by HADDOCK and the rupture forces observed in SMD simulations. This correlation suggests that complexes identified by HADDOCK as possessing heightened binding affinity also exhibit enhanced mechanical stability, as evidenced by the substantial force needed for separation. This integrated approach, amalgamating the iBRAB method for protein preparation, HADDOCK docking predictions, and SMD simulations with optimized pulling parameters, emerges as a valuable tool for elucidating the intricate relationship between binding affinity and mechanical resilience in protein-protein interactions.

Keyword: - *Steered Molecular Dynamic simulation, Protein-protein docking, HADDOCK, iBRAB protocol, Influenza A virus*

1. INTRODUCTION

Influenza A virus (IAV) is recognized as a leading cause of seasonal respiratory illnesses, as well as being responsible for global epidemics that result in millions of deaths worldwide. The earliest documented pandemic is believed to have originated in Russia and reached St. Petersburg in October 1889 [1]. However, the most infamous pandemic, the H1N1 Spanish flu of 1918, began with 550,000 deaths and escalated to an estimated 50 to 100 million deaths worldwide [2]. Subsequently, various pandemics caused by different strains of IAV, including H7N9, H3N2, and H5N1, have occurred [3-6]. Despite the emergence of different threats, the H1N1 virus from the 1918 pandemic remains a potential danger due to its propensity for frequent genetic shifts [7]. Previous studies have led to the development of the *i*BRAB (*in silico* Broad-Reactive Antigen-Binding fragment) protocol, aimed at designing potential therapeutic vaccines against various strains of Influenza A virus (IAV) through computational methods [8]. Building upon research on hemagglutinin-neutralized antibodies, the protocol compiles essential interactive amino acids from antibody-antigen systems to maximize broad-spectrum properties. Initial evaluation using the HADDOCK tool examined the binding affinity of the proposed Fab model targeting hemagglutinin (HA) of different H1N1 Influenza A strains, showing promising broad-reactive potential against the receptor-binding site of HA. However, relying solely on docking scores may not fully reflect the true binding affinity and interaction mechanisms. Consequently, steered molecular dynamics (SMD) simulations emerge as invaluable tools for investigating dynamic biomolecular interactions and understanding binding affinity critical for drug discovery [9].

The SMD technique made its debut in 1997 during the 2nd International Symposium on Algorithms for Macromolecular Modelling, introduced by Professor Klaus Schulten and his team at the University of Illinois (USA) [10]. Before SMD, experimental methods like atomic force microscopy, optical tweezers, biomembrane force probes, and surface force apparatus were utilized to study ligand-receptor or protein complexes, requiring availability of the protein or ligand for the receptor, which posed significant challenges in terms of cost and time [11-18]. SMD emerged as a computational solution, allowing simulation of these interactions with limitless elements. In an SMD simulation, an external vector is applied to one terminus or molecule of a system, while the other terminus or molecule remains fixed, enabling investigation into molecular mechanical stress response. This method employs a virtual damped harmonic spring for applied force, with force-time diagrams used to analyze force distribution at various atomic reaction times, correlated with conformational changes in the investigated proteins or molecules [19]. Over the years, SMD has found wide-ranging applications beyond biomolecule studies, spanning fields like environmental science, ceramic manufacturing, and energy [20-24]. Notably, its role in rational drug design has been extensively explored by research groups worldwide, particularly in understanding interaction mechanisms such as antigen-antibody unbinding processes [25]. During the Covid-19 pandemic, there has been a surge in publications utilizing SMD to study the immune system and design effective therapeutic drugs. Oliveira and colleagues in 2019 investigated the correlation between SMD and experimental AFM methods on antigen-antibody complexes, finding that SMD yielded rupture forces close to AFM data and facilitated identification of key molecular conformations relevant to drug design [26]. Subsequently, SMD has been employed in various projects to elucidate electrostatic interactions, assess the effects of binding mutations, identify critical interactions, understand antibody resistance, and evaluate antibody binding efficacy [27-33].

In this paper, the relationship between rupture forces measured through SMD simulations and scores predicted by previous HADDOCK simulations for protein-protein interactions is accessed. While previous study in protein-ligand system has indicated a general trend where stronger predicted binding scores correlates with a larger force required to separate the molecules in SMD simulations, this correlation is not absolute [34]. Different factors may influence the observed force in SMD, including the direction of molecular pulling, the magnitude of harmony force and rate. By elucidating the nuances of this relationship, we aim to estimate the optimization of pulling force and rate in SMD on our protein-protein systems for correlating with docking score from the HADDOCK.

2. MATERIALS AND METHODS

Model systems. The 3D structures of HA-Fab systems utilized in this study were sourced from two distinct repositories. Initially, ten systems were gathered from the Research Collaboratory for Structural Bioinformatics – Protein Data Bank (RCSB-PDB) database to function as controls (refer to table 1). These systems were selected based on the known interactions between HA and the respective Fab from previous investigations [8]. Additionally, twenty model systems were acquired from the High Ambiguity Driven protein-protein DOCKing (HADDOCK) 2.4 server, resulting from flexible docking between the *i*BRAB model and selected HA proteins [35, 36]. Following clustering analysis, the system exhibiting the highest docking score within the optimal cluster was selected as the representative model for each interaction. Any missing amino acids in the control systems were reconstructed using MODELLER version 9.21, with the interaction poses retained to maintain the corrected binding state [37]. Furthermore, to streamline the structure size for simulation purposes, the HA2 region of the HA protein was omitted, while the HA1 region was retained, as all Fabs bind solely to the receptor-binding site of HA1.

Table -1: List of control systems of antibodies (Abs)/antigen-binding fragments (Fab) and their corresponding Hemagglutinin (HA) proteins of different IAV strains.

No	PDB ID	Fab/Ab	IAV strain	
1	3LZF	2D1 [38]	A/Brevig Mission/1/1918	BM-1/18
2	4GXU	1F1 [39]	A/Brevig Mission/1/1918	BM-1/18
3	4HKX	CH67 [40]	A/Solomon Islands/3/2006	SI-3/06
4	4M5Z	5J8 [41]	A/Nagasaki/09N083/2009	Nag-09N083/09
5	4YK4	641 I-9 [42]	A/Solomon Islands/3/2006	SI-3/06
6	5UG0	H2897 [43]	A/Solomon Islands/3/2006	SI-3/06
7	5UGY	CH65 [44]	A/Solomon Islands/3/2006	SI-3/06
8	5IBL	6639 [45]	A/reassortant/NYMC X-181	X-181
9	6Q0O	H2227 [46]	A/Solomon Islands/3/2006	SI-3/06

10	6Q18	H1244 [46]	A/Beijing/262/1995	Bei-262/95

Steered molecular dynamic simulation. This simulated experiment was executed utilizing GROMACS software, specifically version 2018.3 [47]. The N- and O-termini of each system were left undetermined and retained as obtained from the database or docking method. Parameters derived from the GROMOS96 54A7 force field were applied uniformly across all systems during the simulation process. Short-range nonbonded interactions and long-range electrostatic calculations were configured following established protocols [48]. Each system was subsequently immersed in a triclinic box of simple point charge (SPC) water supplemented with 100nM NaCl and neutralizing counterions to facilitate equilibration. The triclinic box dimensions were adjusted to adhere to the minimum image convention and allow ample space for pulling simulations along the x-axis. This equilibrated structure served as the initial configuration for the subsequent steered molecular dynamics simulation. Equilibration involved a two-step process comprising constant volume (NVT) and constant pressure (NPT) equilibration, with simulation phases lasting 1000 ps each under conditions. Temperature coupling was achieved by separately coupling protein and nonprotein atoms to a temperature bath maintained at 310 K (37°C) using the Berendsen weak coupling method. Pressure was isotropically maintained at 1.0 bar employing a similar weak coupling method. Following equilibration, restraints on HA1 of the hemagglutinin protein were removed, while the heavy and light chains remained immobile for the subsequent pulling simulation. Each HA1 structure was then subjected to pulling along the x-axis for 700 ps using a spring constant optimized for force and rate. The maximum pulling force required to dissociate HA from the Fab was identified as the rupture force and subsequently collected for analysis.

Statistical analysis. The tidyverse package along with ggplot2 within the R tool (utilizing the RStudio interface) was employed for the computation and visualization of all graphs, encompassing the representation of mean, standard deviation, and additional parameters displayed in figures or tables [49-51]. Statistical significance was determined at a p-value threshold of less than 0.05, computed through correlation and regression tests.

3. RESULTS AND DISCUSSION

3.1. The optimum pulling force 1000 kJ/mol/nm^2 and pulling rate 0.005 nm/ps were applied for the SMD simulation of all our systems.

Optimizing the pulling force and rate in SMD simulations is crucial for accurately capturing biomolecular interactions and dissociation events. The pulling force determines the magnitude of mechanical stress applied to the system, while the pulling rate governs the speed at which the molecules are separated. A careful balance between these parameters is necessary to observe the desired molecular behavior effectively [52, 53]. A too high pulling force or rate can lead to artificial disruption of interactions, making it challenging to identify the genuine dissociation process. Conversely, using a pulling force or rate that is too low may result in prolonged simulations or failure to observe dissociation events altogether. By optimizing the pulling force and rate, researchers can enhance the sensitivity and reliability of SMD simulations, allowing for a more accurate characterization of biomolecular interactions and providing valuable insights into biological processes such as ligand-receptor binding, protein unfolding, and complex dissociation. Therefore, optimizing these parameters is essential for obtaining meaningful results and advancing our understanding of biomolecular dynamics and function.

Based on the 3D crystallography structure of one randomly chosen 3LZF as the control system, various pulling velocities and forces were tested on this system to determine the parameters for all other HA-Fab systems. A pulling force of 1000 kJ/mol/nm^2 was applied to select the appropriate parameter combination as a starting point for optimizing pulling velocity. A range of pulling velocities was tested on the 3LZF system, including 0.001, 0.005, 0.01, 0.02, 0.05, 0.08, and 0.1 (nm/ps). Figure 1a illustrates the disparity in capturing rupture force on one system using different pulling velocities. Two areas show linear dependence between rupture force and pulling velocity with $r = 0.998$ and $r = 0.996$, respectively, while the second area confirms the slight increase in rupture force as the pull rate increases. A pulling rate of 0.005 nm/ps was chosen for optimization to capture all interaction changes. Higher pulling velocities increase the magnitude of rupture force. Although higher pull velocities better distinguish rupture force between systems, the resulting peak is overly high leptokurtic, hindering accurate peak identification. Additionally, it may yield artificial force if an extended length is acquired, thus impeding full observation of atomic-level interactions.

Various forces were tested to determine the spring constant for harmonic pulling in SMD at a pulling rate of 0.005 nm/ps, ranging from 100 kJ/mol/nm^2 to 5000 kJ/mol/nm^2 (Fig. 1b). Lower pulling forces may not be sufficient and delay protein dissociation, making the rupture force peak challenging to discern. Conversely, excessive pulling force

leads to an unstable line of cumulative force with excessive noise and fluctuation, hampering rupture force peak identification. Consequently, a pulling force of 1000 kJ/mol/nm^2 was selected for the spring constant in SMD simulation, characterized by a smooth force line and minimal background noise.
The SMD simulation with described parameters was applied to all ten control systems and twenty *i*BRAB models from HADDOCK experiments. In addition, the pulling rate 0.005 nm/ps and spring constant 1000 kJ/mol/nm^2 were applied and kept for all systems. All other setting parameters were as mentioned.

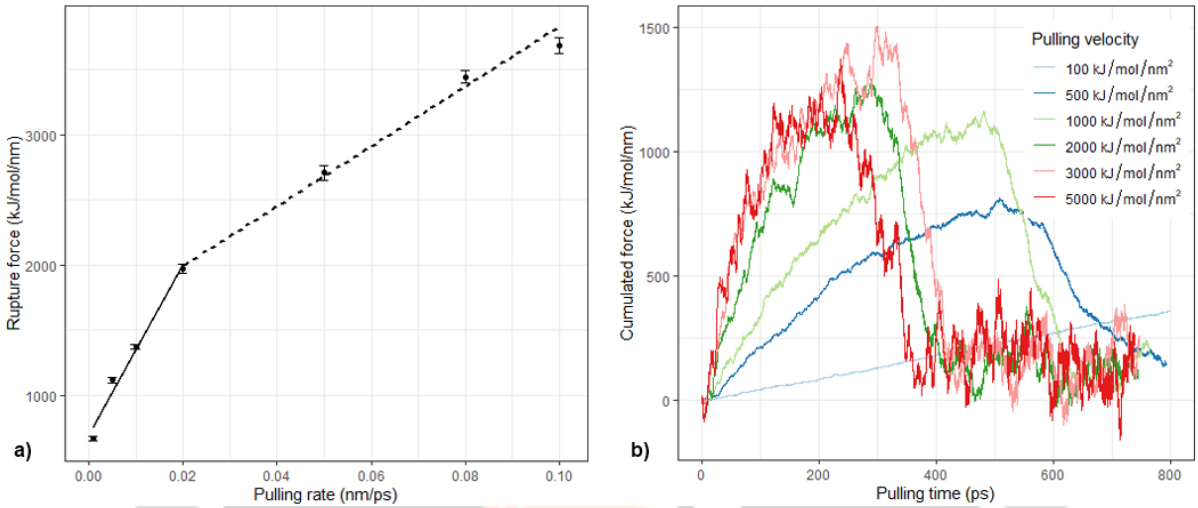

Fig -1: Optimization of pulling rate and pulling velocity in SMD simulation on the control system 3LZF. a) Computed rupture force as a function for different the pulling rate at 1000 kJ/mol/nm^2 spring constant. The error bar was calculated by 15 ps around the peak to estimate the uncertainty. The dashed and dotted lines show two linear parts fitting to a different rate of 0.001-0.02 and 0.02-0.10 nm/ps, respectively. b) The cumulated force of the pulling process using pulling rate 0.005 nm/ps with different applied forces over 800ps as a function for the pulling velocity.

3.2. 2D1 with 1F1, H2897, and 6693 Fabs had good binding with HA protein from A/Brevig Mission/1/1918, A/Solomon Islands/3/2006, and A/reassortant/NYMC X-181, respectively.

Ten control systems obtained from the RCSB database underwent simulation, and their rupture forces were gathered to serve as the control mean. The crystallography technique provides the most authentic protein or protein system structure. Therefore, analyzing the SMD simulation of these systems will establish the control benchmark for comparison with the model systems. Rupture force, identified as the highest force in the simulation, was determined. The mean and standard deviation were computed within 15 ps before and after the peak to ensure the most reliable result. Among the ten controls, the 641 I-9 Fab and its corresponding HA protein in Protein Data Bank (PDB) ID 4YK4 were excluded from the calculation because this crystallography system lacked essential amino acids at the binding site, rendering the obtained SMD data unreliable. With the remaining nine control systems, the 1F1, H2897, and 6693 Fabs exhibited the strongest binding with their respective HA proteins. Notably, the 1F1 Fab has been subject to research aimed at enhancing its therapeutic antibody potential against Influenza A viruses, confirming its efficacy against a broad range of IAV strains. Conversely, the CH67, CH65, H2227, and H1244 Fabs demonstrated the weakest binding and minimal dissociation peak with HA proteins. Although the 5J8 exhibited similarly low binding affinity with its HA protein, the cumulative line indicated clear dissociation between the Fab and HA protein (Fig. 2).
The spring constant of 1000 kJ/mol/nm^2, selected from the evaluation conducted on the 2D1+BM-1/18 system (PDB ID 3LZF), proved suitable for steered molecular simulations involving the 5J8, CH67, H2227, and H1244 Fab systems. This choice yielded a distinct cumulated force line with minimal or no background noise. However, this same spring constant resulted in significant noise levels when applied to other systems, such as the 1F1, CH65, H2897, and 6639 Fab systems. For these systems, a smaller spring constant would be more appropriate, although the results still indicated a noticeable difference in rupture compared to control systems. The average and standard deviation of peak force were calculated for the control systems to facilitate comparison with the model systems, enabling observation of the Fab model's impact on binding with various HA proteins. While previous binding affinity assessments between Fab and HA were exclusively conducted on model systems using the HADDOCK

system, which is capable of calculating their binding affinity, comparable data for the control systems were lacking [8]. Due to the preference for utilizing the most natural binding state from crystallography control systems, the same docking program could not be used to calculate binding affinity. Therefore, employing SMD experiments in this study allows for indirect comparison of the binding efficiency of the Fab models through rupture force analysis.

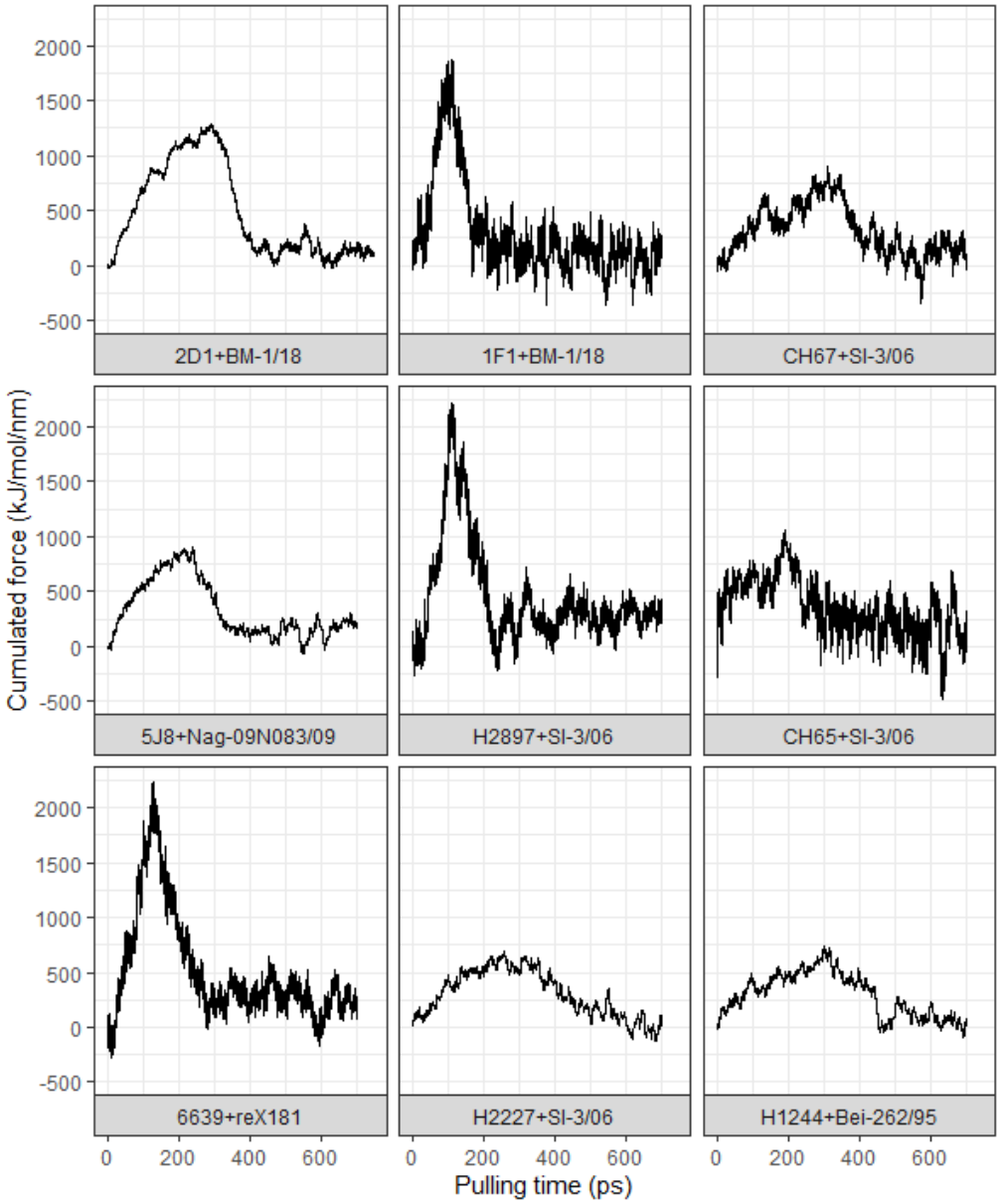

Fig -2: The visible process in the force of the spring over 700 ps of pulling process in nine control systems.

3.3. The rupture force collected from the SMD simulation of all twenty *i*BRAB systems was consistent with a previous study on binding energy between proteins.

The SMD experiment was done on the HADDOCK outputs from the previous study [8]. Different cumulated forces formed in the *i*BRAB model and HA protein systems were recorded and compared. The binding state at the time before pulling is called stage 0. The peak was collected, and rupture force was calculated based on the accumulated force at 15 ps around the peak. These mean and its standard deviation of rupture force were then individually plotted together with the control systems' mean and standard deviation values (Fig.3). The figure shows the rupture force to dissociate different HA from twenty strains of IAV from the *i*BRAB Fab model is within one standard deviation of the mean in control systems, which is a good result in evaluating the broad activity of a Fab on different viral strains.

The HA in Was-05/11 strain required the lowest energy to break the Fab from its; however, there is no sign of significant low force of this strain compared with other strains, such as Jia-ALSI/11 and Kor-01/09. Meanwhile, the strain Bei-262/95 has the HA protein having the highest binding affinity to our model, which required the significant height in force to dissociate the Fab from its. Although the required force to dissociate the *i*BRAB model from HA proteins is not so high as the best binding control system, it shows a stable and similar binding state with different HA proteins from IAV strains. In addition, the SMD rupture force indirectly reveals a better binding affinity of the Fab model than Fabs in control systems.

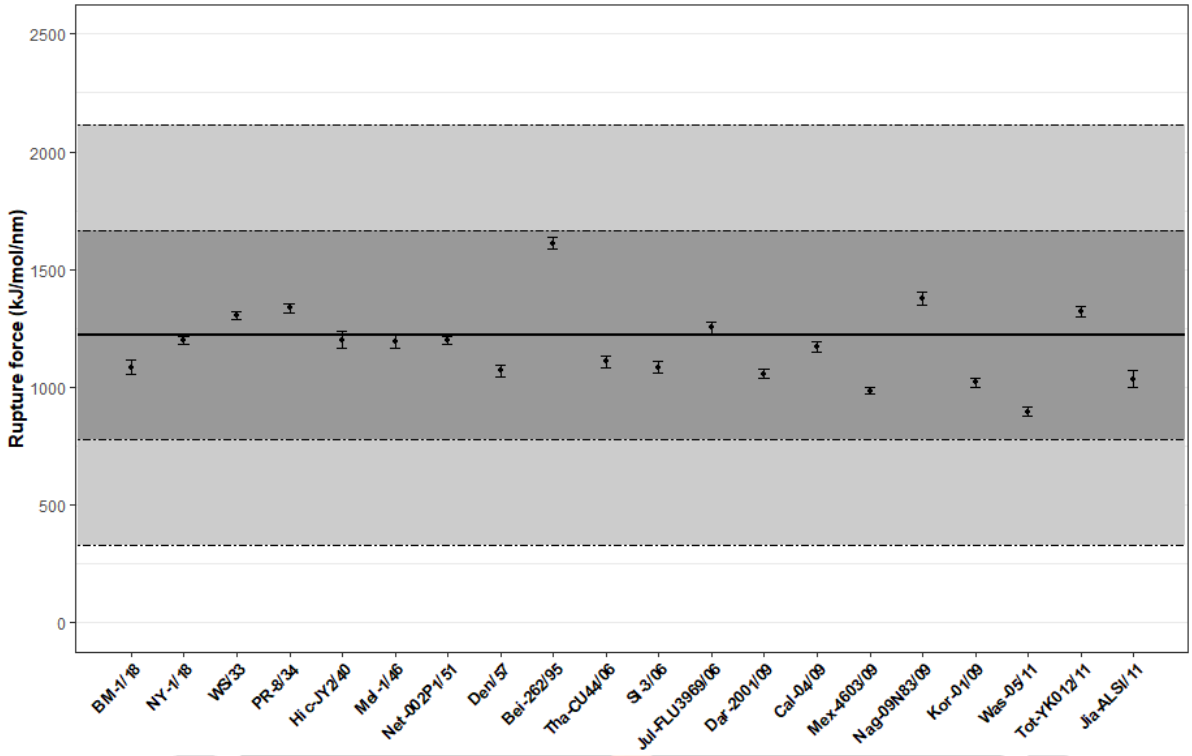

Fig -3: Rupture forces of twenty HA-Fab systems required to dissociate the HA from the *i*BRAB model. The rupture force's mean and standard deviation bar were calculated between 15 ps around the peak. The bold line presents the mean rupture force collected from nine control systems, and the shaded areas stand for one and two standard deviations of the mean, respectively.

To get more detailed information, each trend of cumulated force dissociating the HA proteins from the *i*BRAB Fab model was obtained (Supplementary S01). Within twenty systems of the *i*BRAB Fab model and HA protein, the optimized pull force and rate showed promising results with neat lines and low noise. The difference in rupture force lines can show the difference in the binding behavior of protein-protein systems. Some systems require high accumulated force to pull the HA out of the Fab with a prominent peak. It is explained that the bonds made between Fab and HA are not strong enough to hold the pulling action. The bonds are easily broken with more force build-up when the center of mass increases. This action makes the pulling line more straightforward until the most critical bond is broken. However, several other systems are flexible in forming different bonds when the HA is dissociated from the Fab. The multi-peak line proved the incidence during the SMD simulation. The peak was formed, then another higher peak of cumulated force appeared after a while in Was-05/11 and Tot-YK012/11 systems making the hypothetical statement reliable. Meanwhile, HA protein of Mel-1/46, Hic-HY2/40, and Dar-2001/09 formed with the *i*BRAB Fab model required a particular same accumulated force overtime before breaking from the Fab. A longer bond may be formed between Fab and HA in these systems, which could be reformed or retained at a certain COM distance. Previously, the system of Bei-262/95 and the Fab model has showed the highest binding affinity through the most significant rupture force to dissociate the system. When observing the cumulated line of force formed by this system, the accumulated force straightly increasing shows the strong binding between two proteins; with the dramatically dropped force during a short time, only the short interactive bonds are formed between proteins in this system.

Due to space limitation, in Figure 4, we showed the transition of formed bonds between two selected systems with the highest and lowest rupture force: the Fab model with HAs from Bei-262/95 and Was-05/11 strains, respectively. The simulation was observed every 100 ps from the original pose to 500 ps. During that time, the bonds were broken as the COM longer until there was no bond. As the picture shows, more bonds were formed during about the first 100ps than the original poses, confirming the proteins' flexibility in forming the bonds during the SMD simulation. Through time, the participation of the light chain was less, and the heavy chain made the primary linkage between the Fab and HA until proteins dissociated.

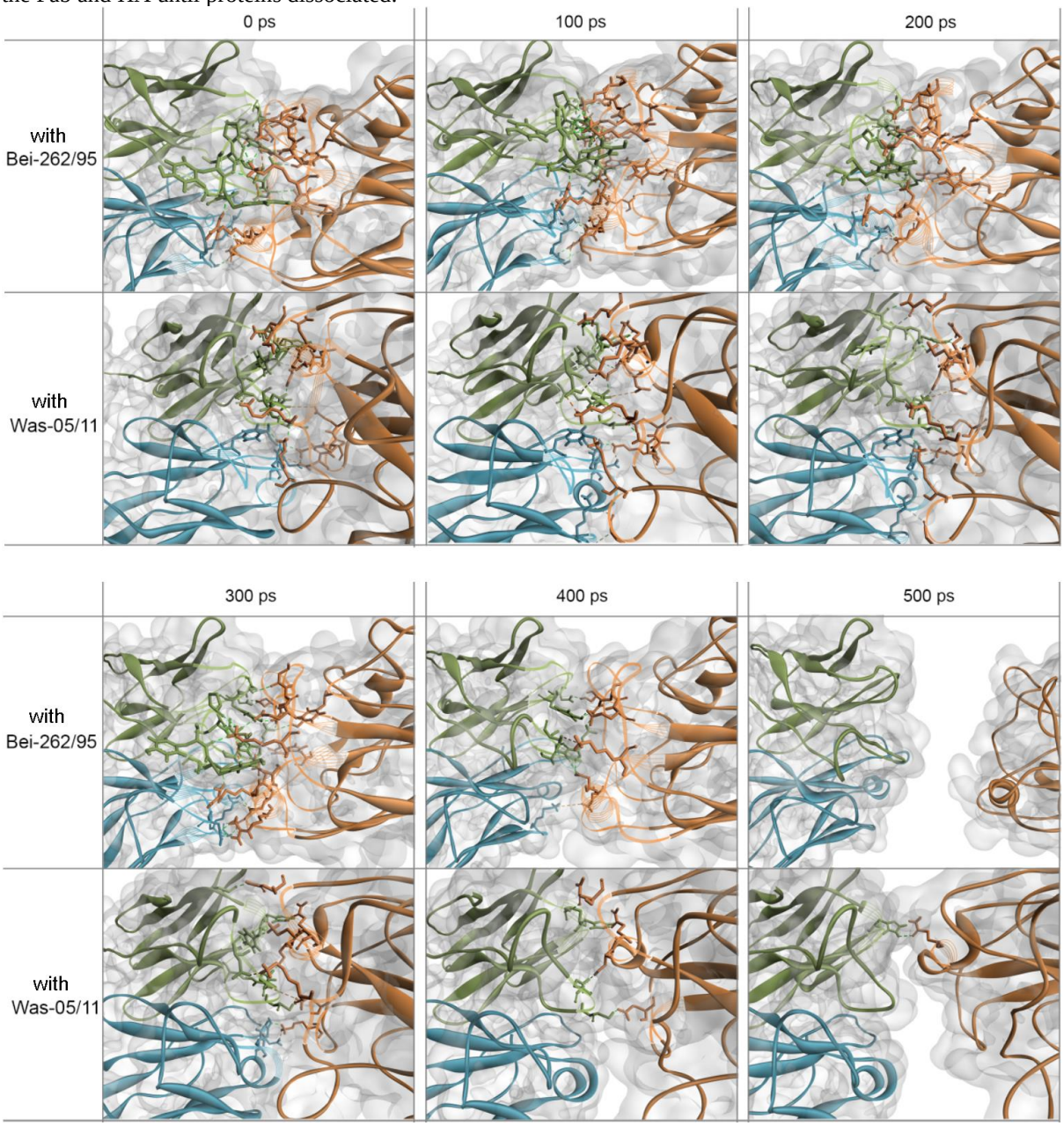

Fig -4: Formed interactive bonds between the *i*BRAB model with Bei-262/95 and Was-05/11 HAs through 500 ps of SMD simulation. The Fab's heavy and light chains are green and blue colors, respectively; the HA protein is red color. The interacted amino acids were displayed in the sticks with their parent colors.

3.4. Docking score predicted by HADDOCK has high correlation with rupture force calculated by SMD

It is essential to comprehend the relationship between docking score and rupture force, particularly in assessing the strength of interactions within protein-protein complexes [54]. Although docking programs like HADDOCK offer

binding affinity predictions through scoring functions, these functions may only partially capture the intricacies of actual dissociation processes. Analyzing the correlation with rupture force, as measured in SMD simulations, provides valuable insights. A robust positive correlation validates the docking predictions, indicating that complexes with low docking scores also exhibit a significant force requirement for separation. Conversely, deviations from this trend highlight limitations in scoring functions or underscore the influence of factors beyond binding affinity, such as conformational flexibility and dissociation pathways. By enhancing the understanding of this correlation, researchers can refine docking methods and gain a more comprehensive understanding of the forces governing protein-protein interactions, thereby facilitating advancements in drug discovery and other areas of molecular biology.

The analysis involved collecting the docking scores from prior HADDOCK experiments and the corresponding rupture forces calculated from SMD simulations conducted on all 20 systems. The data was then plotted to assess the correlation between these two parameters. As depicted in Figure 5, a strong correlation between docking score and rupture force was observed. The coefficient of determination (R^2) was calculated to be 0.97, with the interception set at 0. This high R^2 value suggests that a linear regression model well-explained the relationship between docking score and rupture force. This finding reaffirms the previous suggestion that systems exhibiting high binding affinity, as indicated by low docking scores, also demonstrate a high force requirement for dissociation. This correlation underscores the importance of considering docking score and rupture force in evaluating the strength of molecular interactions within protein-protein complexes.

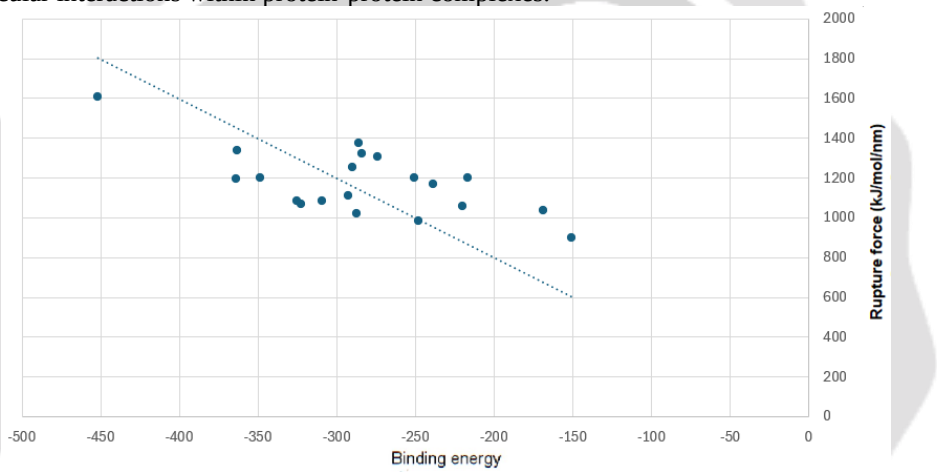

Fig -5: Linear correlation between binding energy and rupture forces of twenty HA-Fab systems. The binding energy was calculated by the HADDOCK tool, while the rupture force were provided by SMD simulation and calculated by mean between 15 ps around the peak.

The analysis has revealed a significant linear correlation between binding energy, as indicated by docking score, and rupture force in our protein-protein complexes. This strong correlation confirms the reliability of previous analysis using only the docking score generated by the HADDOCK tool. This good correlation can inform the development of more accurate predictive models and guide rational design strategies in drug discovery and molecular engineering endeavors.

4. CONCLUSIONS

In conclusion, the results obtained through this study reinforce the importance of optimal parameter optimization in SMD simulations, including the robust linear relationship between rupture force and docking score. Through systematic variation of pulling force and rate, this research determined optimal conditions on which to basis to accurately capture molecular dissociation. Additionally, the strong negative linear relationship between rupture force and docking score confirms the predictive accuracy of docking simulations using HADDOCK in determining binding affinity. Based on the docking score, the researchers can initially predict the binding affinity of protein-protein systems. Afterward, through a measure of rupture force in SMD, they can measure the pulling mechanics of protein-protein systems. This two-pronged approach to measuring the different forces at play in binding events makes it easier to predict protein interactions accurately. Integrating the concepts of the relationship between rupture force and docking score provides a detailed understanding of the subtle equilibrium between binding energy and mechanic strength in molecular interactions. While the former illustrates the metric performance of mechanics of

interacting systems, the latter shows the predictive ability of docking studies. In summary, the relationship between rupture force and docking score correlates well and proves worthwhile for docking studies. Future work should improve the docking algorithms to account for the dynamic nature of proteins and discrepancies between the predicted and measured rupture forces. It would be reasonable to consider other scoring functions and include more empirical data to increase the prediction accuracy. It also includes consideration of the factors affecting mechanical stability in various cell types and computational approaches, such as molecular dynamics simulations. This work will significantly enrich our understanding and provide a foundation for the prospective manipulation of the synthases.

5. ACKNOWLEDGEMENT

We especially appreciate Associate Professor Ly Le for her guidance, supervision and inspiration in finishing this study.

6. REFERENCES

[1] "Is the world ready to respond to the next influenza pandemic?," in *Exploring Lessons Learned from a Century of Outbreaks: Readiness for 2030*, A. V. Ogawa, C. M. Shah, and A. Nicholson, Eds., 2019: The National Academies Press, pp. 7-21.

[2] J. K. Taubenberger and D. M. Morens, "1918 Influenza: the Mother of all pandemics," *Emerging Infectious Diseases*, vol. 12, no. 1, p. 8, 2006, doi: 10.3201/eid1201.050979.

[3] C. H. Stuart-Harris and G. C. Schild, *Influenza: the viruses and the disease.* Edward Arnold, 1958.

[4] N. J. Cox and K. Subbarao, "Global epidemiology of influenza: Past and Present," *Annual Review of Medicine*, vol. 51, pp. 407-421, 2000.

[5] J. C. F. D. Jong, E. C. J. Claas, A. D. M. E. Osterhaus, R. G. Webster, and W. L. Lim, "A pandermic warning?," *Nature*, vol. 389, no. 554, p. 1, 1997.

[6] N. Lee *et al.*, "A major ourbreak of Severe acute raspiratoty syndrome in Hong Kong," *The New England Journal of Medicine*, vol. 348, no. 20, p. 9, 2003.

[7] A. S. Monto and R. G. Webster, "Influenza pandemics: History and lessons learned," in *Textbook of Influenza*, R. G. Webster, A. S. Monto, T. J. Braciale, and R. A. Lamb Eds., 2nd ed.: Wiley Blackwell, 2013, ch. 2, p. 14.

[8] P.-C. Do, T. H. Nguyen, U. H. M. Vo, and L. Le, "iBRAB: In silico based-designed broadspectrum Fab against H1N1 influenza A virus," *PLoS ONE*, vol. 15, p. e0239112, 2020, doi: 10.1371/journal.pone.0239112.

[9] O. M. H. Salo-Ahen *et al.*, "Molecular dynamics simulations in drug discovery and pharmaceutical development," *Processes*, vol. 9, p. 60, 2021, doi: 10.3390/pr9010071.

[10] S. Izrailev *et al.*, "Computational Molecular Dynamics: Challenges, Methods, Ideas," *Lecture Notes in Computational Science and Engineering.*, vol. Vol 4, pp. 39-65, 1997.

[11] L. Moldovan, C. Song, C. Chen, J. Wang, and L. A. Ju, "Biomembrane Force Probe (BFP): Designs, advancements and recent applications to live-cell mechanobiology," *Authorea*, 2023, doi: 10.22541/au.167715770.06231875/v1.

[12] M. T. J. Halma, J. A. Tuszynski, and G. J. L. Wuite, "Optical tweezers for drug discovery," *Drug Discovery Today*, vol. 28, no. 1, pp. 1-12, 2023, doi: 10.1016/j.drudis.2022.103443.

[13] N. E. Kurland, Z. Drira, and V. K. Yadavalli, "Measurement of nanomechanical properties of biomolecules using atomic force microscopy," *Micron*, vol. 43, no. 2-3, pp. 116-128, 2012, doi: 0.1016/j.micron.2011.07.017.

[14] L.-Z. Cheong, W. Zhao, S. Song, and C. Shen, "Lab on a tip: Applications of functional atomic force microscopy for the study of electrical properties in biology," *Acta Biomaterialia*, vol. 99, pp. 33-52, 2019, doi: 10.1016/j.actbio.2019.08.023.

[15] Z. Shao, J. Mou, D. M. Czajkowsky, J. Yang, and J.-Y. Yuan, "Biological atomic force microscopy: what is achieved and what is needed," *Advances in Physics*, vol. 45, no. 1, pp. 1-86, 1996, doi: 10.1080/00018739600101467.

[16] T. O. Pleshakova, N. S. Bukharina, A. I. Archakov, and Y. D. Ivanov, "Atomic Force Microscopy for protein detection and their physicochemical characterization," *International Journal of Molecular Sciences*, vol. 19, no. 4, p. 1142, 2018, doi: 10.3390/ijms19041142.

[17] H. Suna and J. Wang, "Novel perspective for protein–drug interaction analysis: atomic force microscope," *Analyst*, vol. 148, pp. 454-474, 2013, doi: 10.1039/D2AN01591A.

[18] R. Chan and V. Chen, "Characterization of protein fouling on membranes: opportunities and challenges," *Journal of Membrane Science*, vol. 242, no. 1-2, pp. 169-188, 2004, doi: 10.1016/j.memsci.2004.01.029.
[19] H. Lu and K. Schulten, "Steered molecular dynamics simulations of force-induced protein domain unfolding," *Proteins*, vol. 35, pp. 453-463, 1999, doi: 10.1002/(SICI)1097-0134(19990601)35:4<453::AID-PROT9>3.0.CO;2-M.
[20] S. Vassiliev, T. Zaraiskaya, and D. Bruce, "Exploring the energetics of water permeation in photosystem II by multiple steered molecular dynamics simulations," *Biochimica et Biophysica Acta (BBA) - Bioenergetics*, vol. 1817, no. 9, pp. 1671-1678, 2012, doi: 10.1016/j.bbabio.2012.05.016.
[21] K. B. Thapa, K. S. Katti, and D. R. Katti, "Compression of Na–montmorillonite swelling clay interlayer is influenced by fluid polarity: a steered molecular dynamics study," *Langmuir*, vol. 36, no. 40, pp. 11742-11753, 2020, doi: 10.1021/acs.langmuir.0c01412.
[22] J. F. Prins, J. Hermans, G. Mann, L. S. Nyland, and M. Simons, "A virtual environment for steered molecular dynamics," *Future Generation Computer Systems*, vol. 15, no. 4, pp. 485-495, 1999, doi: 10.1016/S0167-739X(99)00005-9.
[23] K. B. Thapa, K. S. Katti, and D. R. Katti, "Influence of the fluid polarity on shear strength of sodium montmorillonite clay: A steered molecular dynamics study," *Computers and Geotechnics*, vol. 158, 2023, doi: 10.1016/j.compgeo.2023.105398.
[24] N. B. Chandar, R. Lo, and B. Ganguly, "Quantum chemical and steered molecular dynamics studies for one pot solution to reactivate aged acetylcholinesterase with alkylator oxime," *Chemico-Biological Interactions*, vol. 223, pp. 58-68, 2014, doi: 10.1016/j.cbi.2014.08.015.
[25] P.-C. Do, E. H. Le, and L. Le, "Steered molecular dynamics simulation in rational drug design," *J. Chem. Inf. Model.*, vol. 58, pp. 1473-1482, 2018, doi: 10.1021/acs.jcim.8b00261.
[26] G. S. Oliveira *et al.*, "Immobilization and unbinding investigation of the antigen-antibody complex using theoretical and experimental techniques," *Journal of Molecular Graphics and Modelling*, vol. 86, pp. 219-227, 2019, doi: 10.1016/j.jmgm.2018.10.012.
[27] H. Nguyen, P. D. Lan, D. A. Nissley, E. P. O'Brien, and M. S. Li, "Electrostatic interactions explain the higher binding affinity of the CR3022 antibody for SARS-CoV-2 than the 4A8 antibody," *B: Biophysical and Biochemical Systems and Processes*, vol. 125, no. 27, pp. 7368-7379, 2021, doi: 10.1021/acs.jpcb.1c03639.
[28] F. Tian *et al.*, "Mutation N501Y in RBD of Spike Protein Strengthens the Interaction between COVID-19 and its Receptor ACE2," *eLife*, 2021, doi: 10.7554/eLife.69091.
[29] E. Taka *et al.*, "Critical interactions between the SARS-CoV-2 spike glycoprotein and the human ACE2 receptor," *B: Biophysical and Biochemical Systems and Processes*, vol. 125, no. 21, pp. 5537-5548, 2021, doi: 10.1021/acs.jpcb.1c02048.
[30] S. T. Ngo, T. H. Nguyen, D.-H. Pham, N. T. Tung, and P. C. Nam, "Thermodynamics and kinetics in antibody resistance of the 501Y.V2 SARS-CoV-2 variant," *RSC Adv.*, vol. 11, pp. 33438-33446, 2021, doi: 10.1039/D1RA04134G.
[31] M. Abidi, R. Soheilifard, and R. H. Ghasemi, "Comparison of the unbinding process of RBD-ACE2 complex between SARS-CoV-2 variants (Delta, delta plus, and Lambda): A steered molecular dynamics simulation," *Molecular Simulation*, vol. 48, no. 18, 2022, doi: 10.1080/08927022.2022.2114599.
[32] H. Nguyen, P. D. Lan, D. A. Nissley, E. P. O'Brien, and M. S. Li*, "Cocktail of REGN antibodies binds more strongly to SARS-CoV-2 than its components, but the Omicron variant reduces its neutralizing ability," *B: Biophysical and Biochemical Systems and Processes*, vol. 126, no. 15, pp. 2812-2823, 2022, doi: 10.1021/acs.jpcb.2c00708.
[33] D. Ray, R. N. Quijano, and I. Andricioaei, "Point mutations in SARS-CoV-2 variants induce long-range dynamical perturbations in neutralizing antibodies," *Chemical Science*, vol. 13, pp. 7224-7239, 2022, doi: 10.1039/D2SC00534D.
[34] J. Gu, H. Li, and X. Wang, "A self-adaptive steered molecular dynamics method based on minimization of stretching force reveals the binding affinity of protein-ligand complexes," *Molecules*, vol. 20, pp. 19236-19251, 2015, doi: 10.3390/molecules201019236.
[35] S. J. d. Vries, M. v. Dijk, and A. M. J. J. Bonvin, "The HADDOCK web server for data-driven biomolecular docking," *Nat. Protoc.*, vol. 5, pp. 883-897, 2010, doi: 10.1038/nprot.2010.32.
[36] G. C. P. v. Zundert *et al.*, "The HADDOCK2.2 web server: User-friendly integrative modeling of biomolecular complexes," *J. Mol. Biol.*, vol. 428, no. 4, pp. 720-725, 2016, doi: 10.1016/j.jmb.2015.09.014.
[37] N. Eswar, D. Eramian, B. Webb, M.-Y. Shen, and A. Sali, "Protein structure modeling with MODELLER," in *Structural Proteomics - High-throughput Methods*, vol. 426, B. Kobe, M. Guss, and T. Huber Eds., (Methods in Molecular Biology™: Humana Press, 2008, pp. 145-159.

[38] R. Xu, D. C. Ekiert, J. C. Krause, R. Hai, J. E. C. Jr., and I. A. Wilson, "Structural basis of preexisting immunity to the 2009 H1N1 pandemic influenza virus," *Science*, vol. 328, pp. 357-360, 2010.
[39] T. Tsibane *et al.*, "Influenza human monoclonal antibody 1F1 interacts with thre major antigenic sites and residues mediating human receptor specificity in H1N1 viruses," *PLoS Pathog.*, vol. 8, no. 12, p. e1003067, 2012.
[40] A. G. Schmidt *et al.*, "Preconfiguration of the antigen-binding site during affinity maturation of a broadly neutralizing influenza virus antibody," *Proc. Natl. Acad. Sci. U.S.A*, vol. 110, no. 1, pp. 264-269, 2013.
[41] M. Hong *et al.*, "Antibody recognition of the pandemic H1N1 influenza virus hemagglutinin receptor binding site," *Virol. J.*, vol. 87, pp. 12471-12480, 2013.
[42] A. G. Schmidt *et al.*, "Viral receptor-binding site antibodies with diverse germline origins," *Cell*, vol. 161, pp. 1-9, 2015.
[43] Y. Liu *et al.*, "CryoEM structure of an influenza virus receptor-binding site antibody-antigen interface," *J. Mol. Biol.*, vol. 429, pp. 1829-1839, 2017.
[44] J. R. R. Whittle *et al.*, "Broadly neutralizing human antibody that recognizes the receptor-binding pocket of influenza virus hemagglutinin," *Proc. Natl. Acad. Sci. U.S.A*, vol. 108, pp. 14216-14221, 2011.
[45] D. D. Raymond *et al.*, "Influenza immunization elicits antibodies specific for an egg-adapted vaccine strain," *Nat. Med.*, vol. 22, pp. 1465-1469, 2016.
[46] K. R. McCarthy, D. D. Raymond, K. T. Do, A. G. Schmidt, and S. C. Harrison, "Affinity maturation in a human humoral response to influenza hemagglutinin," *Proc. Natl. Acad. Sci. U.S.A*, vol. 116, pp. 26745-26751, 2019, doi: 10.1073/pnas.1915620116.
[47] S. Pronk *et al.*, "GROMACS 4.5: a high-throughput and highly parallel open source molecular simulation toolkit," *Bioinformatics*, vol. 29, pp. 845-854, 2013, doi: 10.1093/bioinformatics/btt055.
[48] J. A. Lemkul and D. R. Bevan, "Assessing the stability of Alzheimer's amyloid protofibrils using molecular dynamics," *J. Phys. Chem. B*, vol. 114, pp. 1652–1660, 2010, doi: 10.1021/jp9110794.
[49] M. Campbell, "Essential R Packages: Tidyverse," in *Learn RStudio IDE*: Apress, Berkeley, CA, 2019, pp. 63-72.
[50] H. Wickham *et al.*, "Welcome to the tidyverse," *J. Open Source Softw.*, vol. 4, 2019, doi: 10.21105/joss.01686.
[51] H. Wickham, *Ggplot2: Elegant graphics for data analysis*, 2 ed. (Use R!). Switzerland: Springer International Publishing, 2016.
[52] Y. Pan, R. Qi, M. Li, B. Wang, H. Huang, and W. Ha, "Random acceleration and steered molecular dynamics simulations reveal the (un)binding tunnels in adenosine deaminase and critical residues in tunnels," *RSC Adv.*, vol. 10, pp. 43994-44002, 2020, doi: 10.1039/d0ra07796h.
[53] D. L. Guzmán *et al.*, "Using steered molecular dynamics simulations and single-molecule force spectroscopy to guide the rational design of biomimetic modular polymeric materials," *Polymer*, vol. 49, pp. 3892-3901, 2008, doi: 10.1016/j.polymer.2008.06.047.
[54] L. J. Lapidus, "Exploring the top of the protein folding funnel by experiment," *Current Opinion in Structural Biology*, vol. 23, pp. 30-35, 2013, doi: 10.1016/j.sbi.2012.10.003.